DOI: 10.1002/hep.32738

ORIGINAL ARTICLE





AIF1⁺CSF1R⁺ MSCs, induced by TNF-α, act to generate an inflammatory microenvironment and promote hepatocarcinogenesis

Chen Zong^{1,2} | Yan Meng^{1,2} | Fei Ye^{1,2} | Xue Yang^{1,2} | Rong Li¹ | Jinghua Jiang^{1,2} | Qiudong Zhao^{1,2} | Lu Gao^{1,2} | Zhipeng Han^{1,2} | Lixin Wei^{1,2} ©

Correspondence

Lixin Wei, Tumor Immunology and Gene Therapy Center, Third Affiliated Hospital of Second Military Medical University, 225 Changhai Road, Shanghai, 200438 China. Email: weilixin_smmu@163.com

Abstract

Background and Aims: Increasing evidence suggests that mesenchymal stem cells (MSCs) home to injured local tissues and the tumor microenvironment in the liver. Chronic inflammation is regarded as the major trait of primary liver cancer. However, the characteristics of endogenous MSCs in the inflammatory environment and their role in the occurrence of liver cancer remain obscure.

Approach and Results: Using single-cell RNA sequencing, we identified a distinct inflammation-associated subset of MSCs, namely AIF1⁺CSF1R⁺ MSCs, which existed in the microenvironment before the occurrence of liver cancer. Furthermore, we found that this MSC subgroup is likely to be induced by TNF-α stimulation through the TNFR1/SIRT1 (sirtuin 1) pathway. In a rat primary liver cancer model, we showed that MSCs with high SIRT1 expression (Ad-Sirt1-MSCs) promoted macrophage recruitment and synergistically facilitated liver cancer occurrence by secreting C-C motif chemokine ligand (CCL) 5. Interestingly, depletion of macrophages or knockdown of CCL5 expression in Ad-Sirt1-MSCs attenuated the promotive effect of Ad-Sirt1-MSCs on liver inflammation and hepatocarcinogenesis (HCG). Finally, we demonstrated that SIRT1 up-regulated CCL5 expression through activation of the AKT/HIF1α signaling axis in MSCs.

Conclusions: Together, our results show that MSCs, which are mobilized to the injured site, can be educated by macrophages. In turn, the educated

Abbreviations: AIF1, allograft inflammatory factor 1; AKT, protein kinase B; BECs, bile duct epithelial cells; Casp1, caspase 1; CCL, C-C motif chemokine ligand; CSF1R, colony stimulating factor 1 receptor; Cxc/12, C-X-C motif chemokine ligand 12; DCs, dendritic cells; DEGs, differentially expressed genes; DEN, diethylnitrosamine; GFP, green fluorescent protein; HCG, hepatocarcinogenesis; H&E, hematoxylin–eosin; HIF1α, hypoxia-inducible factor 1 subunit alpha; HPACs, hepatic parenchymal cells; IHC, immunohistochemistry; KEGG, Kyoto Encyclopedia of Genes and Genomes; Lepr, leptin receptor; L-R, ligand-receptor; Mono, monocytes; MSCLCs, mesenchymal stem-cell-like cells; MSCs, mesenchymal stem cells; My, macrophages; Neu, neutrophils; NKs, natural killer cells; MIP3, NLR family pyrin domain containing 3; Nt5e, ecto-5′-nucleotidase; PDGFRβ, platelet-derived growth factor receptor; PPMac, primary peritoneal macrophage; Rbp4, retinol binding protein 4; rTNF-α, recombinant TNF-α; S100a6, S100 calcium-binding protein A6; SCs, stromal cells; scRNA-seq, single-cell RNA sequencing; SD, Sprague–Dawley; Ser473, serine 473; siRNA, small interfering RNAs; SIRT1, sirtuin 1; TNFR1, TNF receptor 1; TUNEL, terminal deoxynucleotidyl transferase dUTP nick end labeling. Supplemental Digital Content is available for this article. Direct URL citations appear in the printed text and are provided in the HTML and PDF versions of this article on the journal's website, www.hepjournal.com.

This is an open access article distributed under the terms of the Creative Commons Attribution-Non Commercial-No Derivatives License 4.0 (CCBY-NC-ND), where it is permissible to download and share the work provided it is properly cited. The work cannot be changed in any way or used commercially without permission from the journal.

Copyright © 2023 The Author(s). Published by Wolters Kluwer Health, Inc.

434 www.hepjournal.com *Hepatology.* 2023;78:434–451

¹Tumor Immunology and Gene Therapy Center, Third Affiliated Hospital of Second Military Medical University, Shanghai, China

²National Center for Liver Cancer, Shanghai, China

MSCs are involved in generating a chronic inflammatory microenvironment and promoting HCG.

INTRODUCTION

HCC remains an important cause of cancer-related mortality worldwide.[1] HCC is relatively insidious and is generally diagnosed at an advanced stage with a poor prognosis. Additionally, heterogeneity in HCC makes targeted treatments less effective. [2] These facts prompted us to focus on preventing HCC. However, the mechanism of liver cancer development is not fully understood, which greatly limits HCC prevention. Primary liver cancer is an inflammation-related cancer, given that >90% of HCCs arise from hepatic injury and inflammation. The inflammatory microenvironment comprises many noncancerous cells, including lymphocytes, mesenchymal stem cells (MSCs), and fibroblasts.[3] Unmasking the characteristics of the tumor-related microenvironment may help us understand the molecular mechanism of hepatocarcinogenesis (HCG).

MSCs are an important component of the chronic inflammatory microenvironment, because of their characteristic of chemotaxis to the damaged site.[4] MSCs have shown great potential in tissue regeneration, wound repair, and maintenance of tissue homeostasis. [5,6] Early research suggested that MSCs were directly involved in damage repair; later, many studies showed that MSCs mainly exert immunosuppressive effects rather than being involved in cell replacement.[7] Furthermore, the immunomodulatory function of MSCs is two-sided and highly plastic. MSCs act as sensors of inflammation and are able to adopt a pro- or anti-inflammatory phenotype by interacting with inflammatory microenvironments.[8,9] Our previous work reported that administration of MSCs at the early stage of HCG can inhibit liver cancer.[10] However, owing to the lack of specific markers to monitor endogenous MSCs, research on the physiological roles of endogenous MSCs is progressing slowly. In fact, it is still unclear whether the immunomodulatory ability of endogenous MSCs is also plastic. The phenotypes and roles of MSCs in HCG remain unknown.

Single-cell RNA sequencing (scRNA-seq), a high-throughput sequencing technology, has developed greatly in recent years. In a recent issue of *Nature*, Ramachandran et al. used scRNA-seq to reveal previously unidentified cell types, which contribute to liver fibrosis progression. [11] The development of scRNA-seq approaches has allowed investigators to discover new cellular states and uncover the genetic heterogeneity of a specific cell type. In a report in *Cell*, the investigators used scRNA-seq data from mouse bone marrow stromal cells to identify *Lepr*⁺ MSCs,

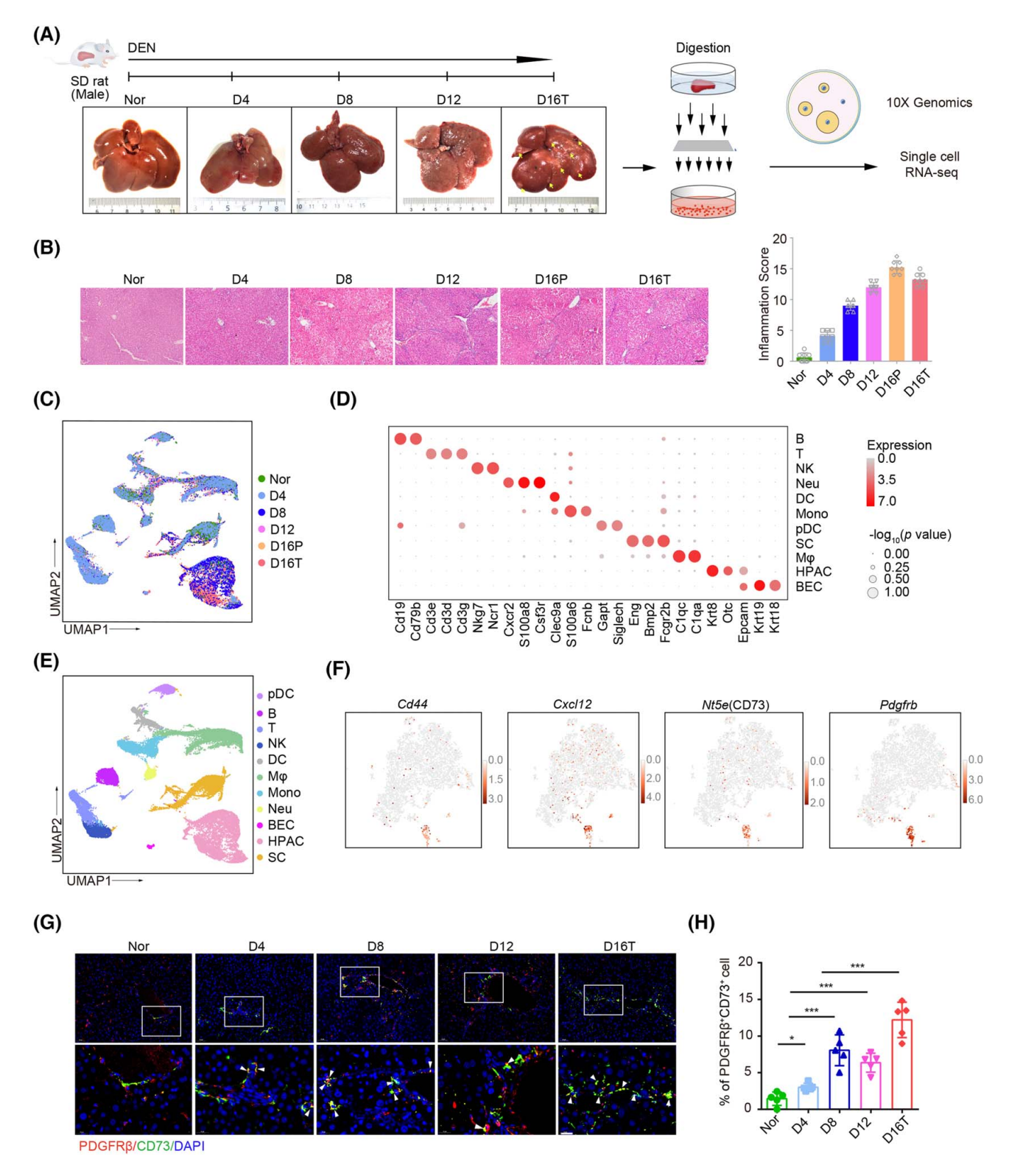
which produce hematopoietic stem cell regulators. The expression profile of one subset of *Lepr*⁺ MSCs suggested differentiation toward the osteoblastic lineage. [12] Additionally, another group used scRNA-seq to identify two distinct subsets of profibrotic bone marrow MSCs in a mouse model of myelofibrosis. [13] Therefore, scRNA-seq may provide a powerful tool for detailed understanding of the status and function of endogenous MSCs under physioand pathological conditions.

Most investigators agree that during HCG, MSCs are mobilized to the injured area where they are exposed to an inflammatory environment. Therefore, in this study, we used scRNA-seq to analyze the properties and verified functions of MSCs during HCG in the rat model. We identified a distinct subset of inflammation-associated MSCs (AIF1+CSF1R+ MSCs), which is present in the inflammatory microenvironment before the occurrence of liver cancer. Then, we further investigated the function of this MSC subset in the development of liver cancer. Our findings reveal an MSC subset that is associated with HCG and shed light on the crosstalk between the chronic inflammatory environment and endogenous MSCs, which will allow us to better understand the mechanism underlying liver cancer occurrence.

MATERIALS AND METHODS

Animals

The rats used in our study were 2- to 3-month-old (weighing 200-300 g) male wild-type Sprague-Dawley (SD) rats, which were purchased from Shanghai Jihui Laboratory Animal Care Co., Ltd. Tnf^{-/-} rats, Tnfrsf1a^{-/-} rats, and Tnfrsf1b^{-/-} rats were all established by the Nanjing Xunqi Biotechnology Company.[14] Briefly, exon 1 of the Tnf gene was targeted to induce DNA deletions with the caspase-9/ single-guide RNA microinjection. Rat tails were collected for identification of mutant alleles by sequence analysis. Tnfrsf1a-/- rats and Tnfrsf1b-/rats were constructed using the same approach. Results showed a 34-bp deletion in exon 2 of the *Tnfrsf1a* gene in *Tnfrsf1a* $^{-/-}$ rats and a 2-bp deletion in exon 3 of the *Tnfrsf1b* gene in *Tnfrsf1b*^{-/-} rats (Figure S3A,B). Tnf, Tnfrsf1a, and Tnfrsf1b genotyping primers are described in Table S1. All animal protocols were approved by the Institutional Animal Care and Use Committee of the Institute of Health Sciences, and all animals received humane care



according to the criteria outlined in the Guide for the Care and Use of Laboratory Animals.

Patient samples

Specimens of liver cancer tissue were obtained from 32 patients with liver cancer who underwent

hepatic resection at the Third Affiliated Hospital of Second Military Medical University from 2001 to 2007. Specimens were analyzed by histological and multicolor immunohistochemistry (IHC) staining. Previous informed consent was obtained, and the study protocol was approved by the Ethics Committee of the Third Affiliated Hospital of Second Military Medical University.

FIGURE 1 Dissecting hepatocarcinogenesis in rats with scRNA-seq. (A) Schematic of the schedule for collection and processing of liver tissue for scRNA-seq and the gross appearance of livers of rats exposed to DEN for 0 weeks (Nor), 4 weeks (D4), 8 weeks (D8), 12 weeks (D12) and 16 weeks (D16). Yellow arrows show tumor nodules. (B) Representative H&E image of liver tissue from DEN-treated rats. The right panel shows the inflammation score of liver tissue. D16T, tumor tissue at DEN16W; D16P, peritumoral tissue at DEN16W. The oval shows tumor tissue in the H&E image. (C) Uniform manifold approximation and projection (UMAP) plot of single cells from livers of rats exposed to DEN. The different time points are indicated by different colors. (D) Classification and identification of cells according to expression of characteristic marker genes. (E) UMAP plot of all cell types (indicated by colors). B, B cells; T, T cells. (F) UMAP plot of the relative expression of each marker gene (Cd44, Cxcl12, Nt5e, and Pdgfrb) from lowest expression (gray dots) to highest expression (red dots) in SCs of panel E. (G) Presence of PDGFRβ+CD73+ cells (white arrows) in liver tissue samples at different stages was detected using IHC staining. Scale bars, 20 μm. (H) Percentage of PDGFRβ+CD73+ cells in the different samples. *p < 0.05; ***p < 0.001. n = 5 for each group. Bmp2, bone morphogenetic protein 2; C1qa, complement C1q A chain; C1qc, complement C1q subcomponent subunit C; Clec9a, C-type lectin domain containing 9A; Csf3r, colony stimulating factor 3 receptor; Cxcr2, C-X-C motif chemokine receptor 2; Eng, endoglin; Epcam, epithelial cell adhesion molecule; Fcgr2b, Fc fragment of IgG receptor Ilb; Fcnb, ficolin B; Gapt, GRB2 binding adaptor protein, transmembrane; Krt, keratin; Ncr1, natural cytotoxicity triggering receptor 1; Nkg7, natural killer cell granule protein 7; Otc, ornithine transcarbamylase; pDC, plasmacytoid dendritic cells; S100a8, S100 calcium-binding protein A8; Siglech, sialic acid-binding immunoglobulin-like lectin

Statistical Analysis

All data are presented as mean \pm SD. Statistical analysis was performed using Prism GraphPad (version 7.0; GraphPad Prism, San Diego, CA). Parameters from treatment groups were compared statistically using unpaired two-tailed Student t test or one-way ANOVA with the *post hoc* Tukey test. Significance was expressed as: $^*p < 0.05$, $^*p < 0.01$, and $^{***}p < 0.001$.

RESULTS

scRNA-seq analysis reveals that mesenchymal stem cell-like cells exist during HCG

In order to create a single-cell atlas during HCG, rats were given 0.1% diethylnitrosamine (DEN; Sigma-Aldrich, St. Louis, MO) in their drinking water to establish a primary liver cancer model. Liver images showed that obvious tumor nodules were observed only at 16 weeks of DEN treatment (DEN16W; Figure 1A, Figure S1A). Inflammatory status was evaluated from hematoxylin-eosin (H&E) images according to grade of necroinflammatory activity. At DEN4W, livers showed mild inflammation. Compared to DEN4W, inflammatory scores increased significantly at DEN8W (D8), then exhibited a slower increase after DEN8W. The inflammation score of tumor tissue at DEN16W (D16T) was decreased compared to that in peritumor tissue at DEN16W (D16P; Figure 1B). We harvested liver tissue samples from rats treated with DEN at 0, 4, 8, 12, and 16 weeks to perform scRNA-seg analysis (Figure 1A). To initially characterize cells in livers at single-cell resolution, we used the 10× Chromium protocol to sequence 39,598 cells from the six rat samples (Figure 1C). Our analysis identified 10 major clusters, which correspond to T cells, B cells, natural killer cells (NKs), dendritic cells (DCs), macrophages (M_{Ψ}) , monocytes (Mono), neutrophils (Neu), bile duct epithelial cells (BECs), hepatic parenchymal cells (HPACs), and stromal cells (SCs),

based on marker gene expression (Figure 1D,E). Interestingly, some stem-cell-related markers, such as Cd44 and ecto-5'-nucleotidase (Nt5e; CD73), were highly expressed in a small proportion of these stromal cells, and other stemness landmarks, such as C-X-C motif chemokine ligand 12 (Cxcl12), S100 calciumbinding protein A6 (S100a6), matrix Gla protein, platelet-derived growth factor receptor (Pdgfra), Pdgfrb, and leptin receptor (Lepr), also exhibited expression patterns similar to Cd44 (Figure 1F, Figure S1B,C). Many of these markers are used to identify MSCs isolated from bone marrow, umbilical cord, and so on.[15,16] Thus, we defined this subgroup of stromal cells as mesenchymal stem-cell-like cells (MSCLCs). To validate the RNAsequencing results at the protein level, we performed immunofluorescence costaining of PDGFRB and CD73 in liver sections and found that a PDGFRβ⁺ CD73⁺ MSCLC subpopulation exists throughout the development of liver cancer (Figure 1G,H).

Annotation of the heterogeneous MSCLCs during HCG

In order to further analyze the heterogeneity of MSCs in HCG, 598 MSCLCs from six liver samples in Figure 1E were subjected to subgroup analysis (Figure 2A). We identified eight subpopulations of MSCLCs with distinct sets of marker genes (Figure 2B). The proportion of MSCLC subgroups in different liver samples is shown in Figure 2C. Then, we noticed that a unique MSCLC subpopulation (cluster 6, MSCLC6) is only enriched in the DEN8W (D8) sample. MSCs in livers at DEN8W are located in the chronic inflammatory microenvironment before tumor formation and are closely related with HCG.[10,17] To delineate the functional profile of MSCLC6, we visualized coordinately expressed gene groups and noticed that cluster 6 was enriched for ontology terms relevant to "inflammatory response" (Figure 2D). Besides common markers, such as Pdafrb or Nt5e (CD73; Figure 1E), MSCLC6 was uniquely characterized by a expression of inflammatory-response-related

genes, namely *Tgfbi*, colony stimulating factor 1 receptor (Csf1r), allograft inflammatory factor 1 (Aif1), Cd74, and retinol binding protein 4 (Rbp4; Figure 2D,E). Csf1r encodes a tyrosine-protein kinase receptor that acts as a cell-surface receptor for CSF1 and IL34 and plays an important role in inflammatory processes.[18] Aif1 encodes allograft inflammatory factor 1, a regulator of macrophage activation and function.[19] MSCLC6 also expressed some inflammasome-related genes, such as NLR family pyrin domain containing 3 (NIrp3), caspase 1 (Casp1), II1b, and II18 (Figure 2F). To validate the existence of this AIF1+CSF1R+ subpopulation (MSCLC6) in vivo, we performed multicolor IHC staining of rat liver tissues and observed that CD73+AIF1+CSF1R+ cells specifically existed at DEN8W, whereas they were barely discovered at other stages of DEN treatment. Similar to CD73+AIF1+CSF1R+ cells, PDGFRβ⁺AIF1⁺CSF1R⁺ cells were also detected mainly at DEN8W (Figure 2G,H, Figure S1D,E). Taking these results together, we considered MSCLC6 to be an AIF1+CSF1R+ population, prominently enriching at DEN8W, and may play a proinflammatory role.

Macrophage-derived TNF- α acts on the AIF1+CSF1R+ MSCLC subgroup through TNF receptor 1

The immunomodulation function of MSCs is not constitutive and must be "licensed" by the inflammatory microenvironment.[7] Thus, in order to find out which immune cells are involved in regulating the immunomodulatory properties of the MSCLC6 subpopulation, we performed multicolor IHC staining to assess the geographical location of MSCLCs relative to different immune cells. Results showed the physical juxtaposition of macrophages (CD68+ cells) and MSCLCs (PDGFRβ+CD73+ cells). T cells, marked by CD3, and neutrophils, marked by myeloperoxidase (MPO), were rarely observed and were located far away from MSCLCs (Figure 3A). This indicated that there might be an interaction between macrophages and MSCLCs. Sequence-based clustering of rat liver macrophages (M_{Φ}) , as shown in Figure 1D, were identified to seven subpopulations (Figure 3B, Figure S2A,B). Importantly, macrophage subpopulation 3 (Mφ3) and macrophage subpopulation 4 (M φ 4) were enriched for ontology terms relevant to inflammatory response, positive regulation of monocyte chemotaxis, and T-cell proliferation in view of special genes. Thus, M ϕ 3 and M ϕ 4 may be regarded as proinflammatory M ϕ . Cells in subpopulation M ϕ 4 were dominant in liver samples from rats treated with DEN for 4 weeks (D4) and, specifically, expressed marker genes like Fc fragment of IgG receptor IIIa (Fcgr3a), folate receptor beta (Folr2), peroxiredoxin 1 (Prdx1), and C-X-C motif chemokine ligand 9 (Cxcl9; Figure 3C,D). In contrast to the M₀4 population, which peaked at D4, the

 $M\phi 3$ population was relatively stable at different time points of DEN treatment (Figure 3D).

Next, we sought to investigate the interactions between macrophages and MSCLCs. We used paired ligand-receptor (L-R) analyses to gain insights into the potential relationships between macrophages and MSCLCs. A set of TNF-related L-R pairs was enriched in the Mφ4 and MSCLC6 subsets, as highlighted in Figure 3E. Notably, only M ϕ 4 was predicted to interact with MSCLC6 (AIF1+CSF1R+ MSCLC) through TNF-based axes (Tnf-Tnfrsf1a, Tnf-Ltbr, and so on; Figure 3E). Among four genes related to TNF signaling (Tnfrsf1a, Tnfrsf1b, Fas, and receptor interacting serine/threonine kinase [Ripk1]), Tnfrsf1a exhibited highest the expression in MSCLC6 (Figure 3F). The ELISA assay further showed that the serum level of TNF- α was maintained at a high level between DEN4W and DEN8W (Figure 3G). Multicolor IHC staining of liver tissue at DEN8W also demonstrated that AIF1 and CSF1R are colocalized with TNFR1 (Figure 3H). All these data suggest that macrophages potentially interact with AIF1+ CSF1R+ MSCLCs (MSCLC6) through TNF-TNFR1.

Continual TNF- α stimulation up-regulates sirtuin 1 in MSCs

In previous studies, we demonstrated that sirtuin 1 (SIRT1) contributes to the immune-enhancement effect of MSCs in the colon cancer liver metastasis model. [20] To determine the mechanism by which TNF- α potentially induces the emergence of AIF1+CSF1R+ MSCLCs (proinflammatory phenotype), we next examined whether TNF-α could up-regulate SIRT1 expression to induce proinflammatory MSCs. Immunofluorescence assays confirmed the colocalization of SIRT1 and proteins in the TNF receptor 1 (TNFR1)-AIF1/CSF1R signaling axis at DEN8W (Figure 4A,B). This suggests that high expression of SIRT1 is closely correlated with CD73⁺AIF1⁺ TNFR1 expression in both and CD73+CSF1R+ To cells. mimic the vivo microenvironment, we used recombinant TNF-α $(rTNF-\alpha)$ to treat MSCs in vitro. $rTNF-\alpha$ (1 ng/ml) significantly up-regulated SIRT1 expression in MSCs after 14 days of treatment (Figure 4C,D). To verify the receptor that rTNF-α acts on, MSCs isolated from Tnfrsf1a^{-/-} rats and Tnfrsf1b^{-/-} rats were treated with rTNF- α to assess SIRT1 expression (Figure 4E, Figure S3A, B). Up-regulation of SIRT1 was abolished in MSCs^{Tnfrsf1a-/-} when exposed to rTNF- α for 14 days, indicating that SIRT1 up-regulation induced by TNF- α is dependent on TNFR1 (Figure 4F,G). To further identify the role of TNF- α on SIRT1 expression in MSCs, $Tnf^{-/-}$ rats were treated with DEN (Figure 4H). In wild-type rats, we found high expression of SIRT1 in CD146+

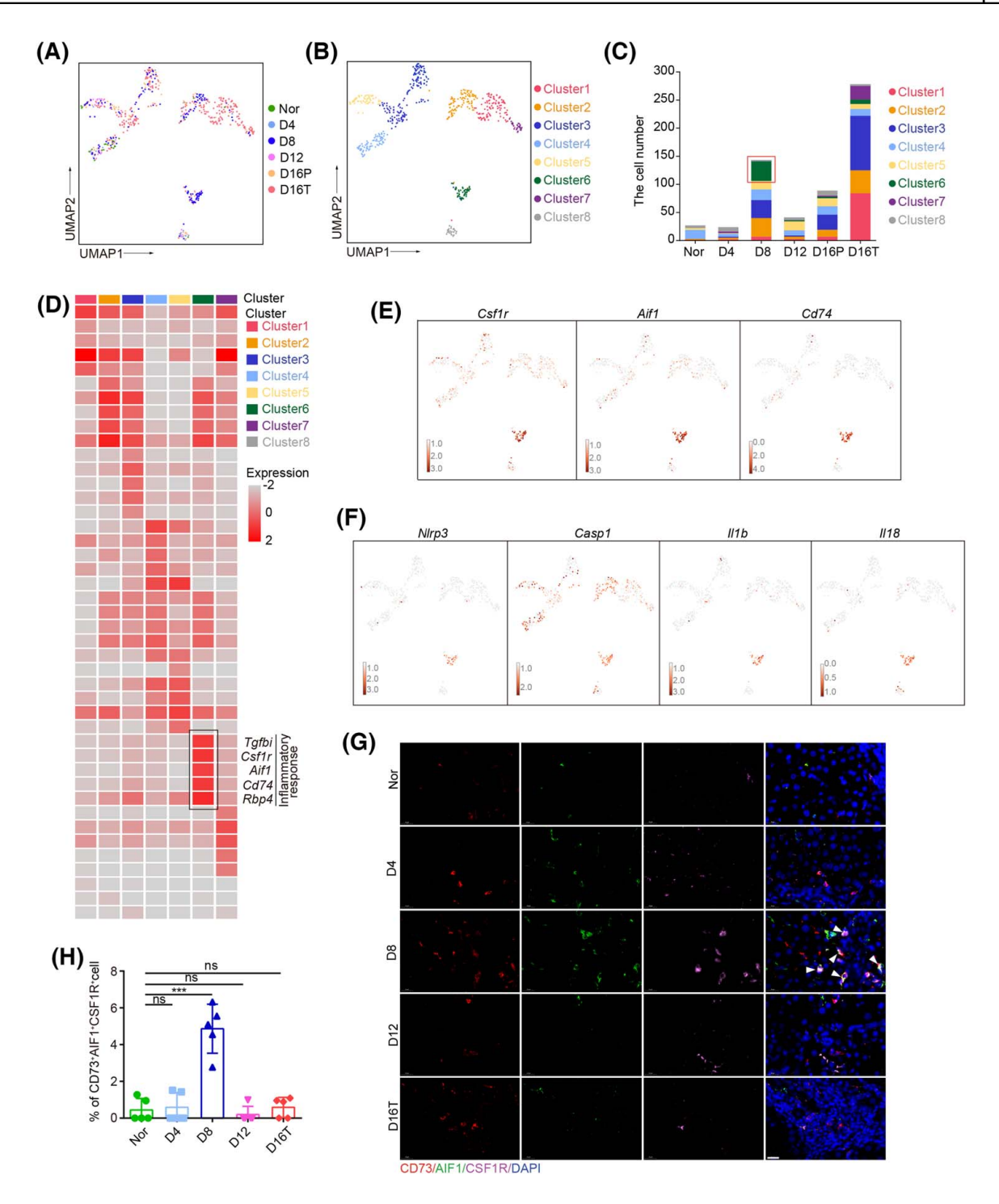


FIGURE 2 Characterization of MSC-like subpopulations. (A) UMAP plot of the MSCLC subpopulations from rats exposed to DEN for different times. Different treatment times are indicated by different colors. (B) UMAP plot of MSCLC subpopulations colored by individual clusters. (C) Stacked bar plots showing the cell composition of clusters in the MSCLC populations from liver samples of rats exposed to DEN for different times. (D) Heatmap of the characteristic markers of each cluster in the MSCLC populations. (E) Expression levels of *Csf1r*, *Aif1*, and *Cd74* were projected onto the UMAP plot from lowest expression (gray dots) to highest expression (red dots). (F) Expression levels of inflammasome-related genes *Nlrp3*, *Casp1*, *Il1b*, and *Il18* were projected onto the UMAP plot from lowest expression (gray dots) to highest expression (red dots). (G) Multicolor staining by IHC of CD73, AIF1, and CSF1R in liver specimens from the Nor, D4, D8, D12, and D16T groups. White arrows show CD73*AIF1*CSF1R* cells. Scale bars, 20 µm. (H) Percentage of AIF1*CSF1R* MSCLC (indicated as CD73*AIF1*CSF1R* cells) in different samples. ***p < 0.001. n = 5 for each group.

cells at DEN8W, which was consistent with the scRNAseq data. In contrast, SIRT1⁺CD146⁺ cells were seldom observed in *Tnf*^{-/-} rats at DEN8W (Figure 4I). Together, our results suggest that continual stimulation with a low level of TNF- α can up-regulate SIRT1 expression in MSCs.

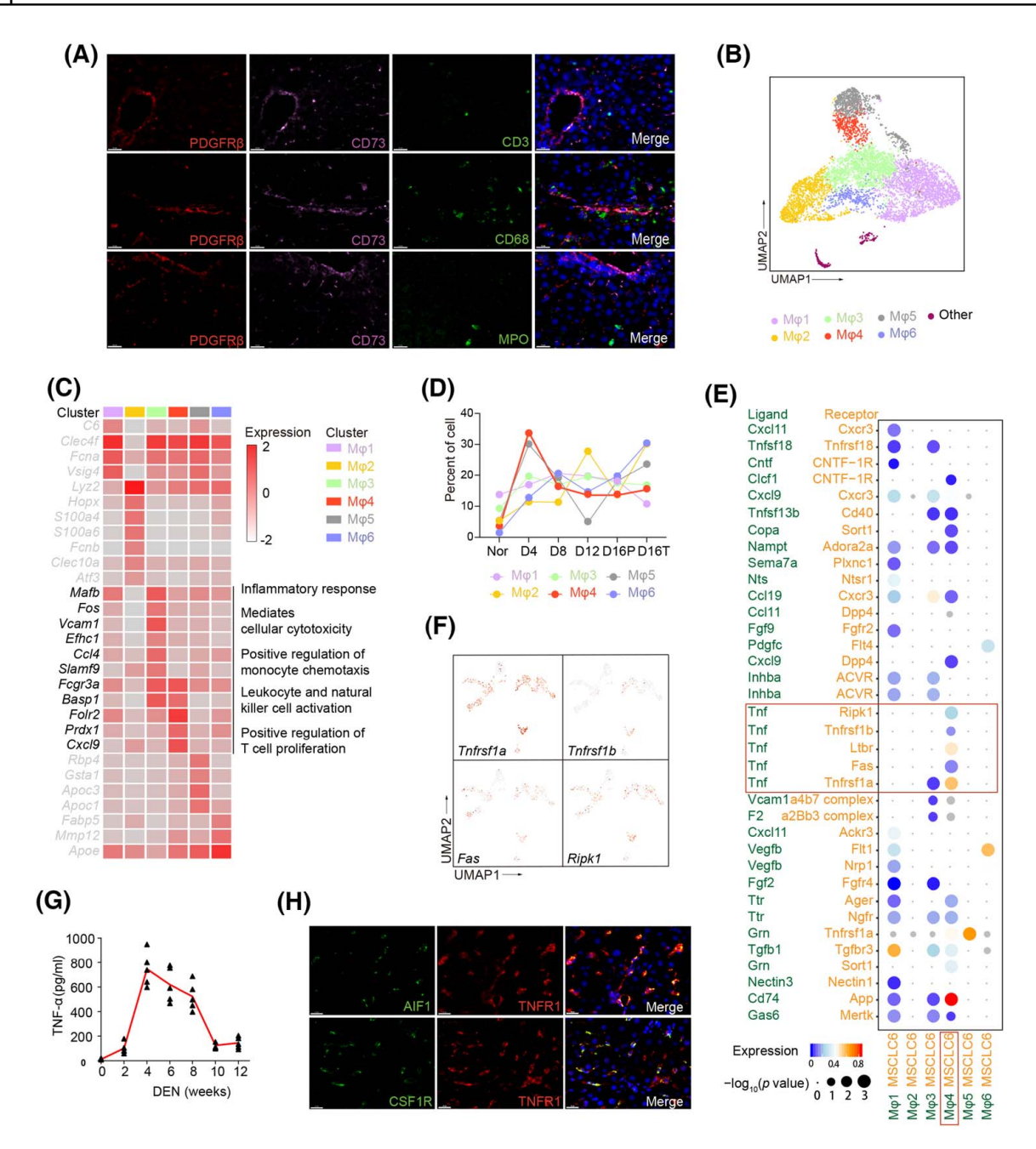


FIGURE 3 Interaction between the MSCLC population and macrophages. (A) Multicolor staining by IHC of PDGFRβ, CD73, CD3, CD68, and MPO. Scale bars, 20 μm. (B) UMAP plot of individual clusters of macrophages. (C) Heatmap of the expression levels of characteristic marker genes for each macrophage cluster. (D) Percentage of cells from the different macrophage subsets in the indicated liver samples. (E) Dot plot of potential L-R interactions between cluster 6 of MSCLC (MSCLC6) and the different macrophage subsets. (F) Expression levels of selected genes (*Tnfrsf1a, Tnfrsf1b, Fas*, and *Ripk1*) in MSCLCs. (G) Level of TNF-α in peripheral blood of DEN-treated rats. *n* = 5 for each group. (H) IHC staining of AIF1, CSF1R, and TNFR1 in liver sections from rats at D8. Scale bars, 20 μm. Apoc1, apolipoprotein C1; Apoc3, apolipoprotein C3; Apoe, apolipoprotein E; Atf3, activating transcription factor 3; Basp1, brain abundant membrane attached signal protein 1; C6, complement C6; Ccl4, C-C motif chemokine ligand 4; Clec4f, C-type lectin domain family 4 member F; Clec10a, C-type lectin domain containing 10A; Efhc1, EF-hand domain containing protein 1; Fabp5, fatty acid binding protein 5; Fcna, ficolin A; Fcnb, ficolin B; Fos, Fos proto-oncogene, AP-1 transcription factor subunit; Gsta1, glutathione S-transferase alpha 1; Hopx, HOP homeobox; Lyz2, lysozyme 2; Mafb, MAF BZIP transcription factor B; Mmp12, matrix metalloproteinase 12; S100a4, S100 calcium-binding protein A4; Slamf9, SLAM family member 9; Vcam1, vascular cell adhesion molecule 1; Vsig4, V-set and immunoglobulin domain containing 4.

The effect of MSCs with high SIRT1 expression on HCG

To explore the role of MSCs with a proinflammatory phenotype in HCG, we constructed MSCs with high

expression of SIRT1 by transduction with adenoviral vector (Ad-Sirt1-MSCs). The transduction efficiency of both Adeno-GFP (green fluorescent protein) and Adeno-Sirt1 was almost 85%, and there was no significant difference between them (Figure S4A).

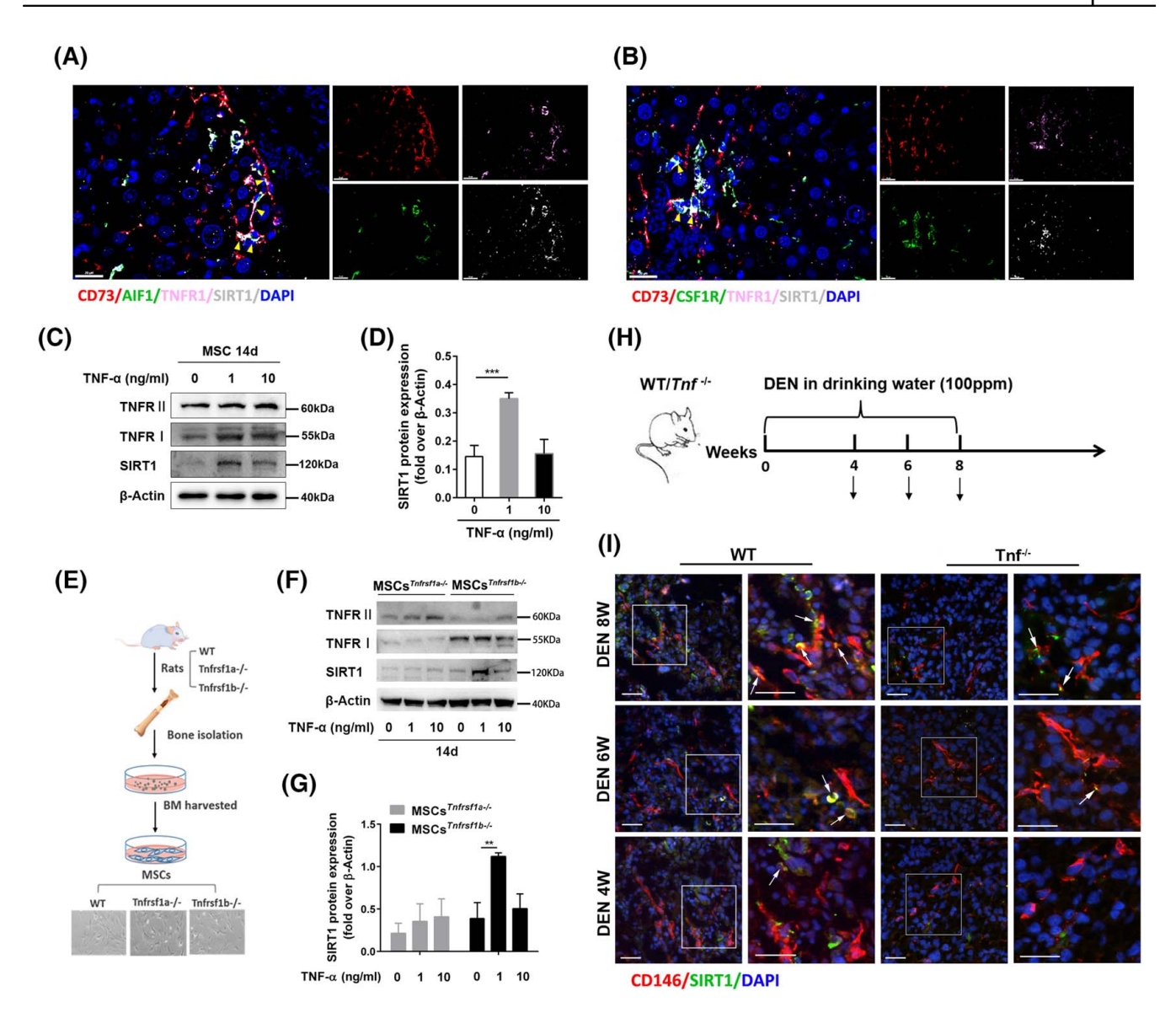
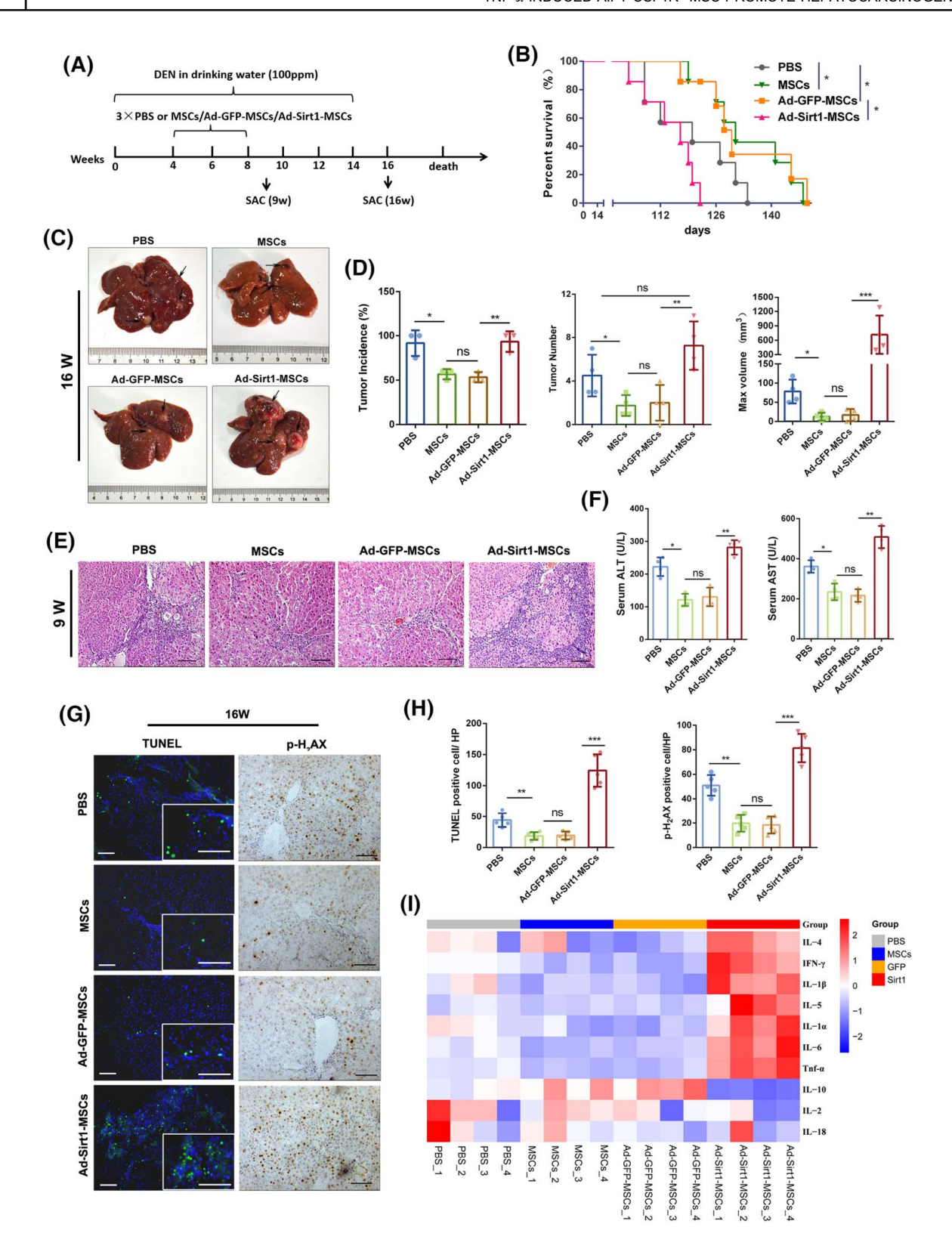


FIGURE 4 TNF- α enhances SIRT1 expression in MSCs through TNFR1. (A) Multicolor IHC staining of CD73, AIF1, TNFR1, and SIRT1 in livers of rats at DEN8W. Yellow arrows indicate CD73*AIF1*TNFR1*SIRT1* cells. (B) Multicolor IHC staining of CD73, CSF1R, TNFR1, and SIRT1 in livers of rats at DEN8W. Yellow arrows indicate CD73*CSF1R*TNFR1*SIRT1* cells. Scale bars, 20 μm. (C) Rat bone-marrow–derived MSCs were treated with recombinant TNF- α (1 or 10 ng/ml) for 14 days, then cell lysates were prepared and subjected to western blotting analysis. (D) Semiquantitative analysis of the western blotting results in panel C. n = 3 for each group. ***p < 0.001. (E) Schematic procedure for isolating MSCs from $Tnfrsf1a^{-/-}$ and $Tnfrsf1b^{-/-}$ SD rats. (F) MSCs^{Tnfrsf1a-/-} and MSCs^{Tnfrsf1b-/-} were treated with recombinant TNF- α (1 or 10 ng/ml) for 14 days, and protein expression levels were determined by western blotting. (G) Semiquantitative analysis of SIRT1 expression examined by western blotting. n = 3 for each group. **p < 0.01. (H) Scheme of WT and $Tnf^{-/-}$ rats exposed to DEN. (I) Expression of SIRT1 in CD146* MSCs was examined by immunofluorescence. Scale bars, 50 μm. Boxed areas are enlarged in the adjacent panels. White arrows indicate CD146*SIRT1* cells. BM, bone marrow; WT, wild type.

Expression of SIRT1 was confirmed in Ad-Sirt1-MSCs by PCR and western blotting assay (Figure S4B, C). Overexpression of SIRT1 in MSCs had no effect on the proliferation and migration capacity of the MSCs (Figure S4D–F). In order to explore the effect of Ad-Sirt1-MSCs on HCG, SD rats with DEN treatment were administered with PBS, MSCs, Ad-GFP-MSCs, and Ad-Sirt1-MSCs (Figure 5A). Ad-GFP-MSCs and Ad-Sirt1-MSCs showed similar migration capacity from tail vein to

liver *in vivo* (Figure S5A). Injection of MSCs and Ad-GFP-MSCs led to prolonged survival and effectively inhibited tumorigenesis, whereas rats in the Ad-Sirt1-MSCs group showed the shortest mean survival time (Figure 5B,C). At DEN12W, obvious tumor nodules were only observed in the Ad-Sirt1-MSCs group (Figure S5B, C). Moreover, the Ad-Sirt1-MSCs group showed a significant increase in the number of detectable HCC nodules and the maximal tumor diameters relative to the other groups at



DEN16W (Figure 5C,D). Accordingly, malignant liver tumors in the Ad-Sirt1-MSCs group displayed strongly increased proliferation, as judged by Ki67 staining, compared with the other groups (Figure S5D, E). These data indicate that Ad-Sirt1-MSCs have a tumor-promoting effect in DEN-induced HCG in rats.

Ad-Sirt1-MSCs aggravate liver injury by enhancing inflammation

The finding that Ad-Sirt1-MSCs can increase the susceptibility of rats to chemical carcinogens prompted us to examine the effect of Ad-Sirt1-MSCs on liver injury

FIGURE 5 MSCs with SIRT1 overexpression (Ad-Sirt1-MSCs) have a tumor-promoting effect in HCG. (A) Schematic diagram for transplantation of MSCs during DEN-induced HCG in rats. PBS or MSCs/Ad-GFP-MSCs/Ad-Sirt1-MSCs (1×10^6) was administered by i.v. injection. (B) Survival curves of rats in the PBS, MSCs, Ad-GFP-MSCs, and Ad-Sirt1-MSCs groups (n = 7). (C) Gross appearance of livers in rats from the four experimental groups. Visible tumors are indicated by the black arrows. (D) Tumor incidence, tumor number, and maximum tumor volume in rats at DEN16W. n = 4 for each group. (E) H&E staining of livers in the different treatment groups at DEN9W. (F) Serum levels of ALT and AST levels were tested at DEN9W. n = 4 for each group. (G) Representative images showing staining of DEN16W liver sections for indicators related to liver injury. (H) Histological semiquantification analysis of TUNEL and p-H₂AX staining. n = 5 for each group. (I) Serum levels of inflammatory factors were detected at DEN9W by the Bio-Plex Pro rat cytokine assay and are displayed as a heatmap. On the x axis, the sample names (e.g., PBS_1, PBS_2, PBS_3, and PBS_4) indicate four different rats at the same time point. Scale bars, 100 μ m. Values are shown as mean \pm SEM (*p < 0.05; **p < 0.01; ***p < 0.001; ns, not significant). ALT, alanine aminotransferase; AST, aspartate aminotransferase; HP, high power field (400×); SAC, sacrifice.

in the early stage of HCG. At DEN9W, the groups receiving MSCs and Ad-GFP-MSCs showed reduced liver damage, as judged by gross examination and biochemical index detection, whereas Ad-Sirt1-MSCs had the opposite effect and led to aggravated liverinjury (Figure 5E,F, Figure S5F). Further examination also showed an increased number of terminal deoxynucleotidyl transferase dUTP nick end labeling (TUNEL)-positive cells and p-H₂AX-positive cells in the Ad-Sirt1-MSCs group, consistent with more severe liver fibrosis in this group (Figure 5G,H, Figure S5F, G). All the data confirmed that administration of Ad-Sirt1-MSCs aggravated DEN-induced liver damage. We next explored how Ad-Sirt1-MSCs exacerbate liver injury. Given the vital role of inflammation in liver injury and HCG, we examined liver inflammation reaction at DEN9W. H&E staining revealed increased infiltration of inflammatory cells in the Ad-Sirt1-MSC group compared to the other two groups (Figure 5E). Accordingly, compared with the other groups, the level of proinflammatory cytokines (IL-4, IL-1β, IFN-γ, TNF-α, and so on) was greatly increased, whereas the level of anti-inflammatory cytokines IL-10 and IL-2 was reduced in the Ad-Sirt1-MSCs group (Figure 51). These results indicate that Ad-Sirt1-MSCs enhanced inflammatory reaction in the liver, instead of exerting immunosuppressive effect.

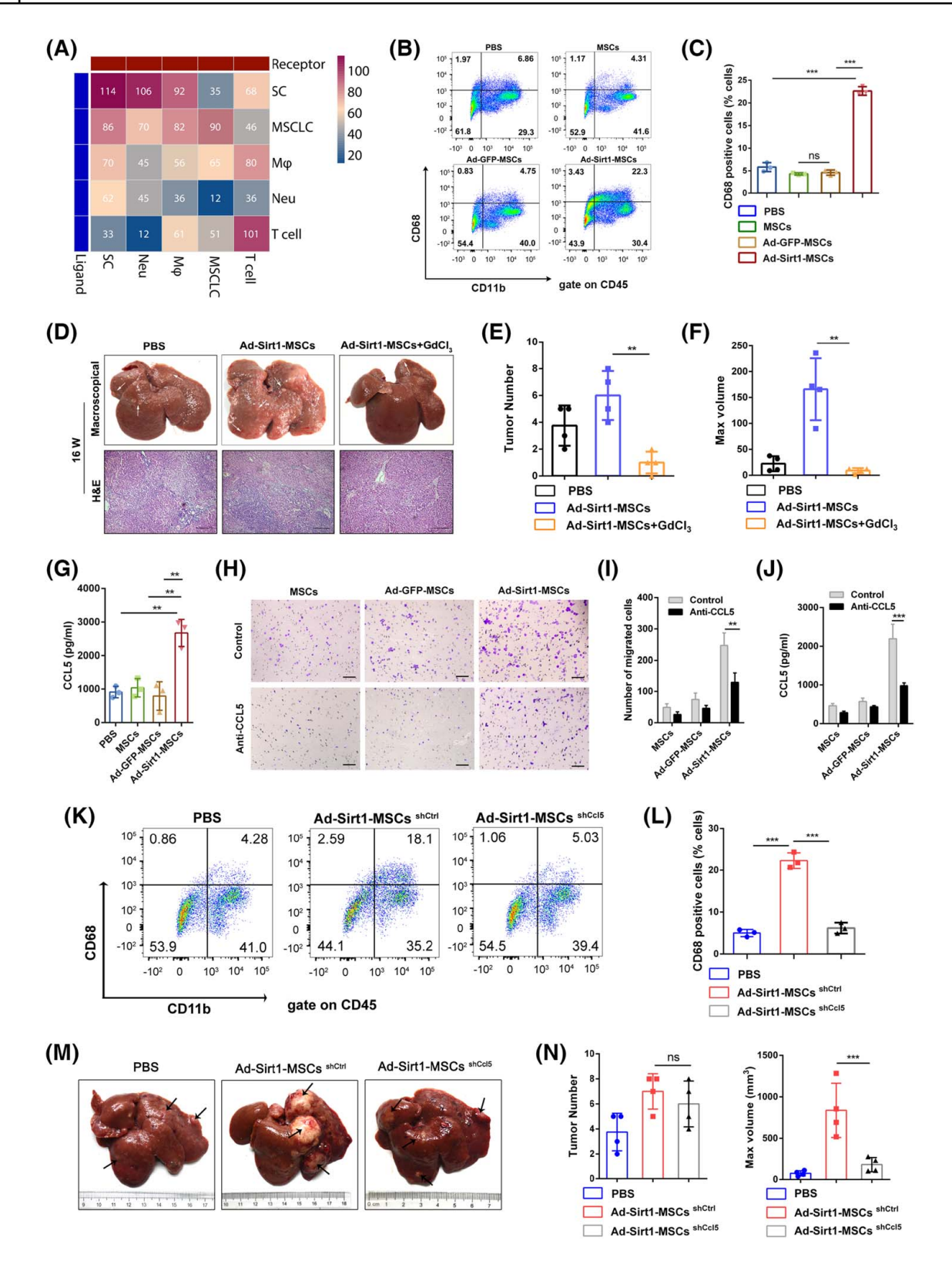
Macrophages are essential for the proinflammatory and tumor-promoting effects of Ad-Sirt1-MSCs

Next, we sought to find out the type of immune cells that Ad-Sirt1-MSCs mainly act on. Based on the scRNA-seq data, we performed paired L-R analyses to gain insights into the potential regulatory relationships between MSCs and liver nonparenchymal cells (including immune cells). Correlation analysis indicated that MSCs interacted more closely with macrophages than with T cells (Figure 6A). Thus, we next verified the effect of Ad-Sirt1-MSCs on macrophages in the liver. The data showed that many more CD11b+CD68+ macrophages infiltrated into livers of the Ad-Sirt1-MSCs group relative to the other three groups, and most of the infiltrated macrophages in the Ad-Sirt1-MSCs group were positive

for CD86, which is regarded as an M1 marker (Figure 6B,C, Figure S6A, B). Collectively, the results indicate that these more abundant macrophages in the Ad-Sirt1-MSC group are predominantly derived from monocytes in the bone marrow, instead of the amplification of resident Kupffer cells. To further confirm whether the tumor-promoting effects of Ad-Sirt1-MSCs rely on macrophages, we depleted macrophages by i.p. injection of GdCl₃ during HCG group^[21] (Figure S6C). Ad-Sirt1-MSCs Immunostaining of CD68 verified the efficiency of GdCl₃-induced macrophage depletion in the liver (Figure S6D, E). Furthermore, macrophage depletion in the Ad-Sirt1-MSCs group resulted in a significant attenuation of inflammatory reaction and liver injury at DEN9W (Figure S6F-H). Accordingly, macrophage depletion attenuated the promotion of HCC by Ad-Sirt1-MSCs. A dramatic decrease in the number of detectable HCC nodules and maximal tumor diameters was observed in the Ad-Sirt1-MSCs + GdCl₃ group relative to the other groups (Figure 6D-F). This indicates that the effect of Ad-Sirt1-MSCs on HCC promotion was dependent on increased infiltration of macrophages.

Ad-Sirt1-MSCs promote macrophage recruitment and migration, but not expansion, in the liver

Considering that macrophage expansion and recruitment are both important factors leading to increased infiltration in the liver, we explored whether Ad-Sirt1-MSCs acted on the proliferation or migration of macrophages. No distinct difference in the level of growth factors, such as granulocyte colony-stimulating factor, colony-stimulating factor, colony-stimulating factor, and VEGF, was observed between the Ad-Sirt1-MSCs group and the other two groups. Notably, higher levels of chemokines, such as C-C motif chemokine ligand (CCL) 3, CCL5, and CCL20, were detected in rats receiving Ad-Sirt1-MSCs (Figure 6G, Figure S7D, E), which implies that Ad-Sirt1-MSCs may play a role in macrophage migration. To further confirm the essential role of Ad-Sirt1-MSCs on macrophage function, Cell Counting Kit-8 and



transwell assays were performed. Ad-Sirt1-MSCs had no obvious effect on the proliferation of rat alveolar macrophage cell line NR8383 (Figure S7A). NR8383 cells are not adherent, so rat primary peritoneal macrophages (PPMac) were used for the migration assay. We found that Ad-Sirt1-MSCs significantly

promoted the migration of PPMac compared with Ad-GFP-MSCs and MSCs (Figure S7B, C). We measured the levels of CCL3, CCL5, and CCL20 in the transwell system and found that the CCL5 level in the Ad-Sirt1-MSCs group was higher than that in other groups (Figure S7F). In summary, the results indicate that

FIGURE 6 CCL5 is involved in the promotive effect of Ad-Sirt1-MSCs on macrophage migration. (A) Number of ligands and receptors in significant L-R pairs in the cell populations. (B) Flow cytometric analysis of CD11b+CD68+ macrophages in livers at DEN9W. (C) Quantitative analysis of the percentage of CD68-positive cells in CD45+ cells isolated from livers. n = 3 for each group. (D) Gross appearance and H&E staining of livers in the PBS, Ad-Sirt1-MSCs, and Ad-Sirt1-MSCs + GdCl₃ groups. (E,F) Number and the maximum volume of tumor nodules were detected in each liver. n = 4 for each group. (G) Serum level of CCL5 was measured at DEN9W. n = 3 for each group. (H) Transwell migration assay for rat primary macrophages treated with anti-CCL5 antibody or not (as control) and cocultured with MSCs for 48 h. (I) Number of migrated cells in the transwell assay. (J) CCL5 levels in the coculture system were measured by ELISA assay. n = 3 for each group. (K) Flow cytometric analysis of CD11b+ and CD68+ cells in livers of rats treated with PBS, Ad-Sirt1-MSCs^{shCtl}, and Ad-Sirt1-MSCs^{shCcl5} at DEN9W. (L) Quantitative analysis of the percentage of CD68+ cells in CD45+ cells isolated from livers of rats at DEN9W. n = 3 for each group. (M) Representative pictures of liver specimens at DEN16W. Black arrows show the visible tumors. (N) Tumor numbers and the maximum tumor volume were measured at DEN16W. n = 4 for each group. Scale bars, 100 μm. Values are shown as mean ± SEM (**p < 0.01; ***p < 0.001; ns, not significant).

CCL5, but not CCL3 and CCL20, may contribute to macrophage migration.

CCL5 is involved in the promotive effect of Ad-Sirt1-MSCs on macrophage migration

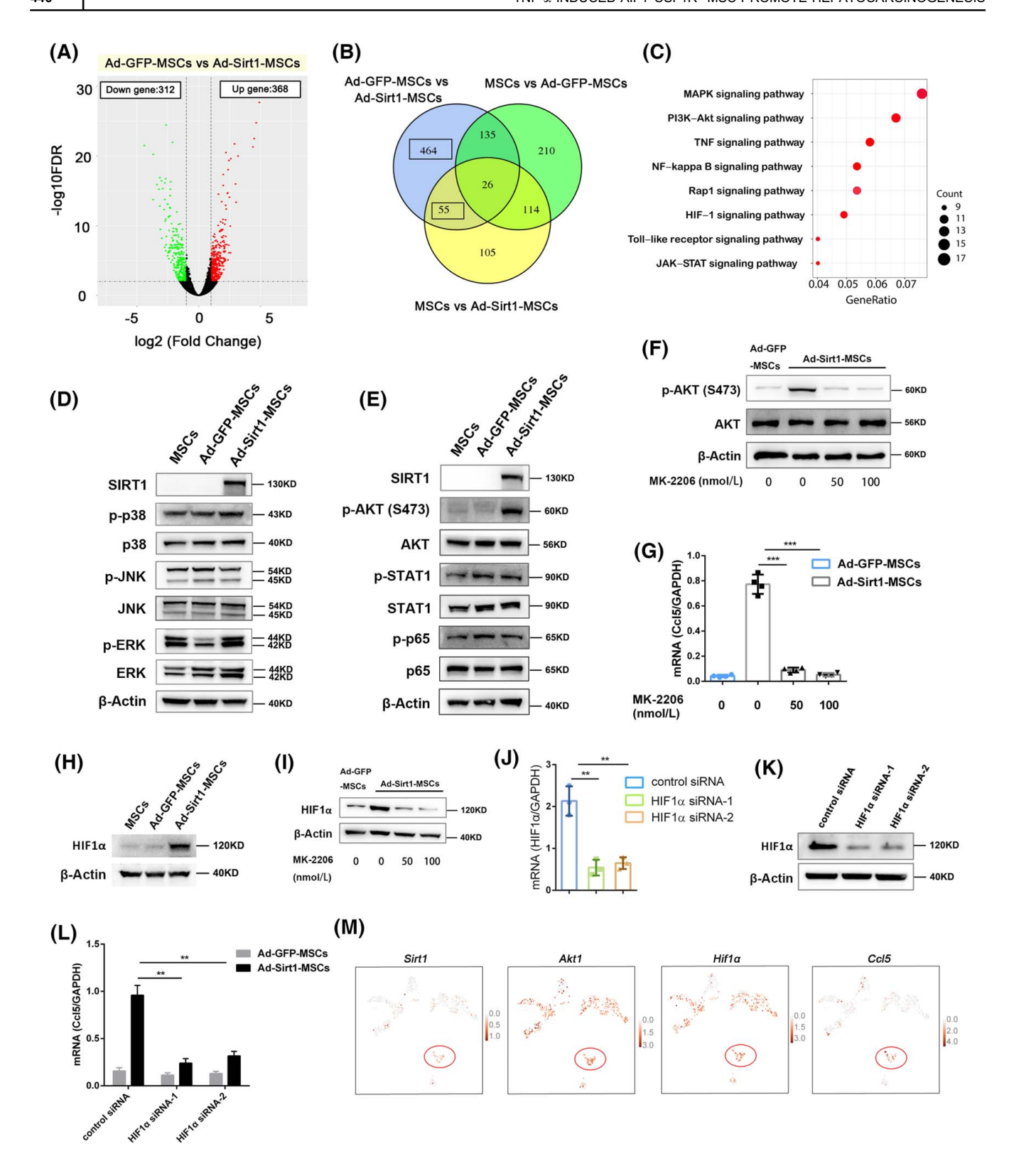
We hypothesized that the high CCL5 level secreted by Ad-Sirt1-MSCs is responsible for macrophage recruitment and migration. To test this hypothesis, a CCL5neutralizing antibody was used in the transwell system. As expected, in the groups receiving no anti-CCL5 (control), the number of migrated PPMac in the Ad-Sirt1-MSCs group was almost 3 times higher than that in the Ad-GFP-MSCs group. The enhancement of PPMac migration by Ad-Sirt1-MSCs was obviously attenuated by anti-CCL5, which indicates that Ad-Sirt1-MSCs probably promote macrophage migration through CCL5 (Figure 6H,I). The ELISA assay confirmed that the CCL5 level in the transwell system was indeed reduced with anti-CCL5 treatment (Figure 6J). To further assess the role of CCL5 in macrophage migration, rat recombinant CCL5 protein was added into the transwell system. The result showed a dose-dependent relationship between CCL5 level and the number of migrated PPMac (Figure S7G). In the process of HCG, the level of CCL5 expression was highly consistent with the number of CD68+ macrophages (Figure S7H). Correlation analysis confirmed that CCL5 expression was correlated with CD68 expression (r = 0.8648, p < 0.01; Figure S7I).

Next, to determine the role of CCL5 in Ad-Sirt1-MSCs-induced macrophage recruitment and tumor progression, we stably reduced the expression of CCL5 in Ad-Sirt1-MSCs using short hairpin RNAs (shRNAs). RT-PCR and ELISA results showed that the shRNA variant, shCcl5 #3, reduced the expression of CCL5 by nearly 70% compared to Ad-Sirt1-MSCs^{shCtrl} (Figure S7J). Then, Ad-Sirt1-MSCs^{shCcl5} were constructed and transplanted into DEN-treated rats. Results showed that the percentage of CD68-positive cells in the liver was significantly decreased in the Ad-Sirt1-MSCs^{shCcl5} group compared to the Ad-Sirt1-MSCs group (Figure 6K,L, Figure S7K). More important, maximal

tumor diameters and relative liver weight were significantly decreased in the Ad-Sirt1-MSCs^{shCcl5} group, although no significant difference in the number of detectable tumors (> 1 mm) was observed between the Ad-Sirt1-MSCs^{shCcl5} and Ad-Sirt1-MSCs^{shCcl5} groups (Figure 6M,N). These results suggest that CCL5 deficiency alleviates the promotive effect of Ad-Sirt1-MSCs on HCC development. However, the number of tumors was still increased by nearly 1.5-fold in the Ad-Sirt1-MSCs^{shCcl5} group compared with the PBS group (Figure 6N). We speculate that this is probably because the CCL5 level in the Ad-Sirt1-MSCs^{shCcl5} group is higher than the basal expression in the PBS group.

SIRT1 up-regulates CCL5 expression through the protein kinase B/hypoxia-inducible factor 1 subunit alpha signaling pathway

To get a better understanding of the mechanism by which Sirt1 up-regulates CCL5 expression, we performed RNA profiling to identify which signaling pathways are induced by SIRT1 in MSCs and then may induce CCL5 expression. Two independent samples of MSCs, Ad-GFP-MSCs and Ad-Sirt1-MSCs, were collected and then RNA-seg analysis was performed. Results showed a total of 680 differentially expressed genes (DEGs) in Ad-Sirt1-MSCs compared to Ad-GFP-MSCs (Figure 7A). Among them, 368 were up-regulated and 312 were down-regulated. The Venn diagram in Figure 7B represents the degree of overlap for genes found to be up- or down-regulated in Ad-Sirt1-MSCs or Ad-GFP-MSCs relative to MSCs (controls). We found that 161 of the above-mentioned 680 Ad-GFP-MSCs versus Ad-Sirt1-MSCs DEGs overlapped with MSCs versus Ad-GFP-MSCs DEGs. In order to exclude the effect of pure adenovirus transduction on the RNA expression profile in MSCs, we chose to use only the remaining 519 DEGs in our subsequent analysis. The 519 DEGs were examined by Kyoto Encyclopedia of Genes and Genomes (KEGG) pathway analysis, and eight signaling pathways were significantly enriched (Figure 7C). Furthermore, western blotting assays were



used to confirm the key signaling pathway(s) regulated by SIRT1 in MSCs. SIRT1 significantly promoted the phosphorylation of protein kinase B (AKT), but not other candidate pathways, such as the mitogen-activated protein kinase, NF-κB, and Janus kinase/signal transducer and activator of transcription

signaling (Figure 7D,E). Exposing Ad-Sirt1-MSCs to MK-2206 (AKT inhibitor) decreased the phosphorylation of AKT and the expression of *Ccl5* mRNA (Figure 7F,G). This indicates that the SIRT1-induced up-regulation of CCL5 expression depends on AKT phosphorylation.

FIGURE 7 SIRT1 up-regulates CCL5 expression through the AKT/HIF1α signaling axis in MSCs. (A) Volcano plot showing DEGs for Ad-Sirt1-MSCs versus Ad-GFP-MSCs at 48 h after adenovirus transduction. (B) Venn diagram analysis of DEGs after pair-wise comparison of three experimental groups. (C) KEGG enrichment analyses of 519 DEGs from Ad-Sirt1-MSCs versus Ad-GFP-MSCs. The eight most significantly enriched KEGG pathways are illustrated as bubbles. (D) Protein expression related to MAPK signaling was measured by Western blotting analysis. (E) Western blotting analyses to detect levels of proteins related to the AKT and NF-κB signaling pathways. (F) Ad-Sirt1-MSCs were treated with AKT inhibitor (MK-2206), and phosphorylation of AKT (Ser473) was assayed by western blotting analysis. (G) Ccl5 mRNA expression was analyzed in Ad-Sirt1-MSCs treated with AKT inhibitor. (H) HIF1α protein expression was assessed by western blotting assay. (I) Ad-Sirt1-MSCs were treated with AKT inhibitor (MK-2206), and HIF1α protein expression was assayed by western blotting. (J) Real-time PCR analysis of HIF1α mRNA expression in different groups. (K) Western blottings were used to confirm knockdown of HIF1α at the protein level after 48-h transduction. (L) Ccl5 mRNA level was measured in both Ad-GFP-MSCs and Ad-Sirt1-MSCs after transduction with $HIF1\alpha$ siRNA. (M) UMAP plot showing the relative expression of Sirt1, Akt1, Hif1 α , and Ccl5 from lowest expression (gray dots) to highest expression (red dots) in the MSCLC subpopulations of Figure 2B. The red oval indicates Sirt1, Akt1, Hif1α, and Ccl5 expression in MSCLC6 (AIF1+CSF1R+ MSCs) according to scRNA-seq data. AKT, protein kinase B; ERK, extracellular signal-regulated kinase; GAPDH, glyceraldehyde-3-phosphate dehydrogenase; JAK, Janus kinase; MAPK, mitogen-activated protein kinase; p-p38, phosphorylated p38; p-p65, phosphorylated p65; p-AKT, phosphorylated AKT; p-ERK, phosphorylated ERK; PI3K, phosphoinositide 3-kinase; p-JNK, phosphorylated JNK; p-STAT1, phosphorylated STAT1; Rap1, Ras-related protein 1; STAT, signal transducer and activator of transcription.

Furthermore, to determine the effector of SIRT1mediated activation of AKT signaling, we investigated the role of hypoxia-inducible factor 1 subunit alpha (HIF1 α). HIF1 α is regarded as a transcription factor of Ccl5, [22] and the HIF1 α pathway is enriched in KEGG analysis of the DEGs, as shown in Figure 7C. We demonstrated that overexpression of SIRT1 in MSCs up-regulated HIF1 α expression, and the AKT inhibitor, MK-2206, reduced HIF1α expression in Ad-Sirt1-MSCs (Figure 7H,I). These data indicate that AKT acts upstream of HIF1α. We previously showed that SIRT1 up-regulates CCL5 expression in MSCs to promote macrophage infiltration. To determine whether HIF1α affects CCL5 expression in MSCs, HIF1α small interfering RNAs (siRNAs) were transfected into Ad-Sirt1-MSCs. HIF1α deficiency significantly diminished Ccl5 expression in Ad-Sirt1-MSCs compared to the control group (Figure 7J-L). Then, we examined the expression patterns of Sirt1, Akt, Hif1 α , and Ccl5 at the single-cell level in rat liver tissue. In MSCLC6 (AIF1+CSF1R+ MSCs), the patterns of Akt, Hif1 α , and Ccl5 expression were extremely similar to those of Sirt1 (Figure 7M). Together, these results imply that SIRT1 regulates CCL5 expression through the AKT-HIF1α signaling pathway.

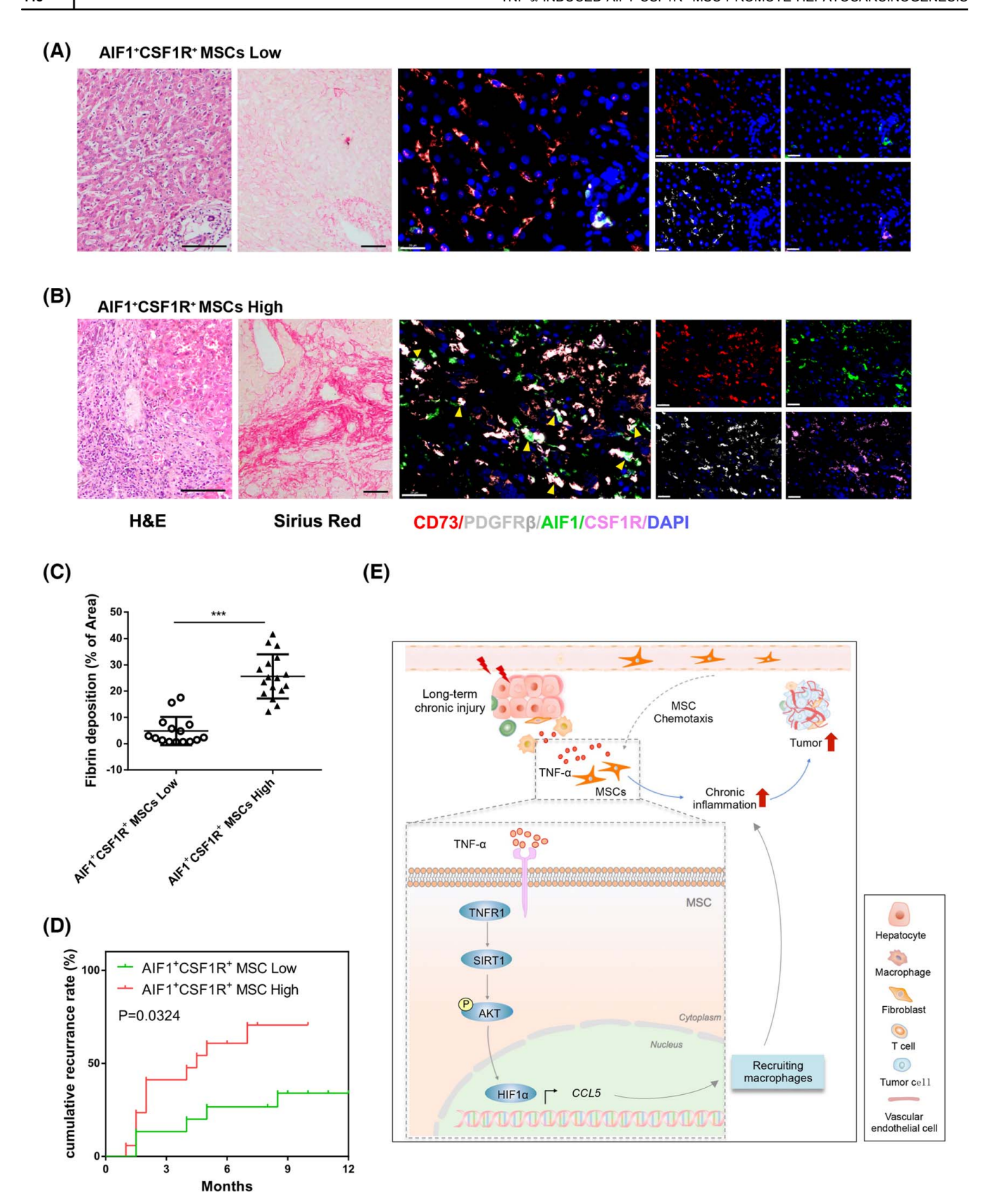
AIF1⁺CSF1R⁺ MSCs in peritumoral tissue correlate with hepatic fibrosis and recurrence of liver cancer

Next, to explore the potential association of AIF1+CSF1R+ MSCs in peritumoral tissue of patients with clinical outcomes, we performed multicolor IHC staining of CD73, PDGFR β , AIF1, and CSF1R on tissue microarrays containing 38 primary liver cancer specimens with long-term clinical follow-up data. Consistent with our findings in rats, we observed the presence of inflammation-related AIF1+CSF1R+ MSCs (shown as CD73+PDGFR β +AIF1+CSF1R+ cells) in peritumoral tissue of patient samples. Then, according to the

number of AIF1+CSF1R+ MSCs, patients were divided into two groups: AIF1+CSF1R+ MSCs Low (15 of 32; 46.9%) and AIF1+ CSF1R+ MSCs High (17 of 32; 53.1%; 6 patient specimens with suboptimal staining were excluded; Figure 8A,B). Furthermore, we quantified the fibrin deposition in the two groups, and found that the AIF1+CSF1R+ MSCs High group had the most fibrin deposition in the specimens, whereas the AIF1+CSF1R+ MSCs Low group had minimal collagen deposition (Figure 8C). This indicates that the abundance of AIF1+CSF1R+ MSCs is associated with liver fibrosis. Furthermore, patients in the AIF1+CSF1R+ MSCs High group had a higher 1-year tumor recurrence rate compared to patients in the AIF1+CSF1R+ MSCs Low group (1-year cumulative tumor recurrence rate: 64.7% vs. 33.3%, log rank test, p = 0.0324; Figure 8D). This finding indicates that the number of AIF1+CSF1R+ MSCs in peritumoral tissue may be useful in predicting the recurrence of liver cancer.

DISCUSSION

Accumulating evidence suggests that both endogenous and exogenous MSCs can migrate to inflamed tissue and participate in tissue repair.[23,24] However, the functional contributions of MSCs during the development of liver cancer are far from fully understood. Our previous studies showed that early infusion of MSCs has a suppressive effect on DEN-induced liver cancer.[10] However, the physiological roles of endogenous MSCs were not verified owing to a lack of specific markers to monitor MSCs in vivo.[25] Recently, Zhou et al. found that the LepR is a marker highly enriched in MSCs from bone marrow. [26] Fate-mapping showed that LepR⁺ cells are the main source of bone formation. Additionally, Kramann et al. reported that GLI family zinc finger 1 (Gli1) is a marker of MSCs in adult tissue. Gli1+ MSCs are regarded as progenitors of vascular smooth muscle cells in vascular remodeling.[27] However, MSCs are a complex mixture of cells, and it is



difficult to understand the overall characteristics and functions of MSCs with single-marker tracing. Here, we used scRNA-seq analysis to unmask the functions of MSCs during HCG. scRNA-seq is a popular method for transcriptome expression analysis at the single-cell level, which can give insight into the existence and behavior of different cell types and cell subsets. [28] By scRNA-seq, we identified a unique

FIGURE 8 Number of AIF1⁺CSF1R⁺ MSCs in peritumoral tissue is correlated with hepatic fibrosis and recurrence of liver cancer. (A,B) Left two panels: Sections of human peritumoral liver tissues were stained with H&E and Sirius Red. Scale bars, 100 μm. Right panels: immuno-fluorescence images of human peritumoral liver tissues stained with antibodies against CD73, PDGFRβ, AIF1, and CSF1R. Nuclei were detected with DAPI. Yellow arrows show the AIF1⁺CSF1R⁺ MSCs. Scale bars, 20 μm. (C) Fibrin deposition (% area) was analyzed based on Sirius Red staining in patient tissue in the Low and High groups in panel A. Values are shown as mean ± SEM (***p < 0.001). (D) Kaplan–Meier curves showing the cumulative recurrence rate for liver cancer patients in the Low and High groups. (E) Schematic model of the mechanism by which AIF1⁺CSF1R⁺ MSCs, stimulated by TNF-α, contribute to construction of a chronic inflammatory microenvironment, which promotes HCG. In summary, MSCs are educated by the chronic inflammatory environment to promote inflammation and HCG through the TNFR1/SIRT1/HIF1α/ CCL5 signaling axis.

inflammation-associated AIF1*CSF1R* MSC subset, which exists in the inflammatory microenvironment before liver cancer occurrence. In fact, the number of cells captured by single-cell sequencing technology is limited, especially for MSCs; therefore, some MSC subsets may still await discovery.

Indeed, the immunomodulatory effects of MSCs need to be "licensed" by inflammatory stimulation. Furthermore, the role of MSCs in immunomodulation is plastic: MSCs can be rendered immunosuppressive in the presence of strong inflammation, whereas weak inflammation induces MSCs to exert an immuneenhancement effect.[29,30] Here, we found that only macrophages were physically juxtaposed MSCLCs, and macrophages may interact with AIF1+CSF1R+ MSCs through Tnf-Tnfrsf1a. TNF-α plays an important role in the survival, migration, and immunoregulation properties of MSCs.[31,32] A recent study reported that TNF-α-stimulated MSCs secreted more IL-8 and exhibited enhanced recruitment of polymorphonuclear granulocytes.[33] Here, we showed that another chemokine, CCL5, is regulated in MSCs by TNF-α through TNFR1/SIRT1 and, subsequently, promotes macrophage infiltration in the liver. CCL2/C-C motif chemokine receptor 2 signaling is the major chemotactic axis involved in the recruitment of monocytes and macrophages.[34,35] In our study, we also observed a high level of CCL2 in the liver, but there was no significant difference between the group treated with Ad-Sirt1-MSCs and the other groups. In support of our findings, studies have reported the specific effect of CCL5 on macrophage recruitment in both adipose tissue and the tumor microenvironment.[36,37] Of course, we do not rule out the role of CCL2 in macrophage migration: We noticed that antibody neutralization of CCL5 could not completely inhibit macrophage migration, and this may be attributed to the activity of CCL2.

SIRT1, a well-studied deacetylase, is involved in functional regulation of the immune response, including macrophages.^[38,39] SIRT1 is regarded as a key regulator of macrophage self-renewal and apoptosis.^[40,41] Furthermore, increasing evidence shows that SIRT1 overexpression can promote macrophage activation and M1 polarization in the context of liver inflammation.^[42,43] MSCs also possess immune regulation capacity and are closely related to immune

cells. Here, we showed that SIRT1 is highly expressed in proinflammatory MSCs (AIF1+CSF1R+ MSCs) after TNF- α stimulation and promotes CCL5 expression and macrophage migration by phosphorylating AKT at serine 473 (Ser473). Similarly, Liu et al. reported that SIRT1 promoted Rictor transcription, which triggered the phosphorylation of AKT at Ser473 in primary hepatocytes and liver cancer cells. [44] Furthermore, by using coimmunoprecipitation and glutathione S-transferase pull-down assays, researchers also verified that SIRT1 directly interacts with histone H3 and phosphorylates H3^{T3} in osteosarcoma cells. [45] These outcomes demonstrate that SIRT1, apart from its histone deacetylase and methylase activity, also exhibits histone phosphoryl transferase activity.

In summary, we identified that a subset of AIF1⁺CSF1R⁺ MSCs, with high expression of SIRT1, exists in the inflammatory microenvironment. We investigated the influence of MSCs with high SIRT1 expression (Ad-Sirt1-MSCs) in HCG. We showed that Ad-Sirt1-MSCs promote macrophage infiltration and liver cancer initiation and progression, which might be mediated by the secretion of CCL5. Furthermore, SIRT1 up-regulates CCL5 expression in MSCs mainly through the AKT/HIF-1 α signaling pathway. Our findings reveal an MSC subset that is associated with HCG and shed light on the crosstalk between the chronic inflammatory environment and endogenous MSCs. These discoveries will allow us to better understand the immunoregulation capacity of endogenous MSCs and the mechanism underlying liver cancer.

AUTHOR CONTRIBUTIONS

Lixin Wei, Chen Zong, and Yan Meng designed the study. Chen Zong, Yan Meng, Xue Yang, Fei Ye, and Rong Li developed the methodology, performed the experiments, and analysis the data. Chen Zong and Yan Meng wrote the manuscript. Jinghua Jiang and Zhipeng Han contributed to the data analysis and manuscript revision. Qiudong Zhao and Lu Gao provided technical assistance. All authors have read and approved the final manuscript.

ACKNOWLEDGMENT

We thank Hangjie Zhang for establishing the preliminary experiment scheme. We also thank Isabel Hanson Scientific Writing for editing services.

FUNDING INFORMATION

This project was supported by the National Key R&D Program of China (Grant No. 2018YFA0107500); National Natural Science Foundation of China (Grant No. 81872243, 81972599, 82073032, 82073037, and 82173276); and the Shanghai Municipal Health Bureau (Grant No. 20214Y0013).

CONFLICTS OF INTEREST

The authors declare that there are no conflicts of interest.

DATA AVAILABILITY STATEMENT

Part of the data is being uploaded, and the GEO number generated later will be added to the article. And some raw data required to reproduce these findings cannot be shared at this time as the data also forms part of an ongoing study.

ORCID

Lixin Wei https://orcid.org/0000-0002-9526-5348

REFERENCES

- Siegel RL, Miller KD, Jemal A. Cancer statistics, 2017. CA Cancer J Clin. 2017;67:7–30.
- D'Souza S, Lau KC, Coffin CS, Patel TR. Molecular mechanisms of viral hepatitis induced hepatocellular carcinoma. World J Gastroenterol. 2020;26:5759–83.
- Ringelhan M, Pfister D, O'Connor T, Pikarsky E, Heikenwalder M. The immunology of hepatocellular carcinoma. Nat Immunol. 2018;19:222–32.
- Liu Y, Yang X, Jing Y, Zhang S, Zong C, Jiang J, et al. Contribution and mobilization of mesenchymal stem cells in a mouse model of carbon tetrachloride-induced liver fibrosis. Sci Rep. 2015;5:17762.
- Zhang S, Chuah SJ, Lai RC, Hui JHP, Lim SK, Toh WS. MSC exosomes mediate cartilage repair by enhancing proliferation, attenuating apoptosis and modulating immune reactivity. Biomaterials. 2018;156:16–27.
- Kou M, Huang L, Yang J, Chiang Z, Chen S, Liu J, et al. Mesenchymal stem cell-derived extracellular vesicles for immunomodulation and regeneration: a next generation therapeutic tool? Cell Death Dis. 2022;13:580.
- Wang Y, Chen X, Cao W, Shi Y. Plasticity of mesenchymal stem cells in immunomodulation: pathological and therapeutic implications. Nat Immunol. 2014;15:1009–6.
- 8. Chen X, Gan Y, Li W, Su J, Zhang Y, Huang Y, et al. The interaction between mesenchymal stem cells and steroids during inflammation. Cell Death Dis. 2014;5:e1009.
- Waterman RS, Tomchuck SL, Henkle SL, Betancourt AM. A new mesenchymal stem cell (MSC) paradigm: polarization into a proinflammatory MSC1 or an immunosuppressive MSC2 phenotype. PLoS One. 2010;5:e10088.
- Zong C, Zhang H, Yang X, Gao L, Hou J, Ye F, et al. The distinct roles of mesenchymal stem cells in the initial and progressive stage of hepatocarcinoma. Cell Death Dis. 2018;9:345.
- Ramachandran P, Dobie R, Wilson-Kanamori JR, Dora EF, Henderson BEP, Luu NT, et al. Resolving the fibrotic niche of human liver cirrhosis at single-cell level. Nature. 2019;575: 512–8.
- Baryawno N, Przybylski D, Kowalczyk MS, Kfoury Y, Severe N, Gustafsson K, et al. A cellular taxonomy of the bone marrow

- stroma in homeostasis and leukemia. Cell. 2019;177(7): 1915–932 e16.
- Leimkühler NB, Gleitz HFE, Ronghui L, Snoeren IAM, Fuchs SNR, Nagai JS, et al. Heterogeneous bone-marrow stromal progenitors drive myelofibrosis via a druggable alarmin axis. Cell Stem Cell. 2021;28(4):637–52 e8.
- Jing Y, Sun K, Liu W, Sheng D, Zhao S, Gao L, et al. Tumor necrosis factor-alpha promotes hepatocellular carcinogenesis through the activation of hepatic progenitor cells. Cancer Lett. 2018;434:22–32.
- Melzer C, Jacobs R, Dittmar T, Pich A, von der Ohe J, Yang Y, et al. Reversible growth-arrest of a spontaneously-derived human MSC-like cell line. Int J Mol Sci. 2020;21(13):4752.
- Srinivasan A, Sathiyanathan P, Yin L, Liu TM, Lam A, Ravikumar M, et al. Strategies to enhance immunomodulatory properties and reduce heterogeneity in mesenchymal stromal cells during ex vivo expansion. Cytotherapy. 2022;24:456–72.
- Sun K, Guo XL, Zhao QD, Jing YY, Kou XR, Xie XQ, et al. Paradoxical role of autophagy in the dysplastic and tumorforming stages of hepatocarcinoma development in rats. Cell Death Dis. 2013;4:e501.
- Lin W, Xu D, Austin CD, Caplazi P, Senger K, Sun Y, et al. Function of CSF1 and IL34 in macrophage homeostasis, inflammation, and cancer. Front Immunol. 2019;10:2019.
- Egana-Gorrono L, Chinnasamy P, Casimiro I, Almonte VM, Parikh D, Oliveira-Paula GH, et al. Allograft inflammatory factor-1 supports macrophage survival and efferocytosis and limits necrosis in atherosclerotic plaques. Atherosclerosis. 2019;289: 184–94.
- Ye F, Jiang J, Zong C, Yang X, Gao L, Meng Y, et al. Sirt1overexpressing mesenchymal stem cells drive the anti-tumor effect through their pro-inflammatory capacity. Mol Ther. 2020; 28:874–88
- Li XF, Chen C, Xiang DM, Qu L, Sun W, Lu XY, et al. Chronic inflammation-elicited liver progenitor cell conversion to liver cancer stem cell with clinical significance. Hepatology. 2017; 66:1934–51.
- Yeligar SM, Machida K, Tsukamoto H, Kalra VK. Ethanol augments RANTES/CCL5 expression in rat liver sinusoidal endothelial cells and human endothelial cells via activation of NF-kappa B, HIF-1 alpha, and AP-1. J Immunol. 2009;183: 5964–76.
- Pajarinen J, Lin T, Gibon E, Kohno Y, Maruyama M, Nathan K, et al. Mesenchymal stem cell-macrophage crosstalk and bone healing. Biomaterials. 2019;196:80–9.
- Oh EJ, Lee HW, Kalimuthu S, Kim TJ, Kim HM, Baek SH, et al. In vivo migration of mesenchymal stem cells to burn injury sites and their therapeutic effects in a living mouse model. J Control Release. 2018;279:79–88.
- Shi Y, Wang Y, Li Q, Liu K, Hou J, Shao C, et al. Immunoregulatory mechanisms of mesenchymal stem and stromal cells in inflammatory diseases. Nat Rev Nephrol. 2018; 14:493–507.
- Zhou BO, Yue R, Murphy MM, Peyer JG, Morrison SJ. Leptinreceptor-expressing mesenchymal stromal cells represent the main source of bone formed by adult bone marrow. Cell Stem Cell. 2014;15:154

 –68.
- Kramann R, Schneider RK, DiRocco DP, Machado F, Fleig S, Bondzie PA, et al. Perivascular Gli1+ progenitors are key contributors to injury-induced organ fibrosis. Cell Stem Cell. 2015;16:51–66.
- Papalexi E, Satija R. Single-cell RNA sequencing to explore immune cell heterogeneity. Nat Rev Immunol. 2018;18: 35–45.
- Naji A, Eitoku M, Favier B, Deschaseaux F, Rouas-Freiss N, Suganuma N. Biological functions of mesenchymal stem cells and clinical implications. Cell Mol Life Sci. 2019;76:3323–48.

 Zhang T, Wang Y, Li Q, Lin L, Xu C, Xue Y, et al. Mesenchymal stromal cells equipped by IFNα empower T cells with potent antitumor immunity. Oncogene. 2022;41(13):1866–81.

- 31. Nakao Y, Fukuda T, Zhang Q, Sanui T, Shinjo T, Kou X, et al. Exosomes from TNF-α-treated human gingiva-derived MSCs enhance M2 macrophage polarization and inhibit periodontal bone loss. Acta Biomater. 2021;122:306–24.
- Bai X, Xi J, Bi Y, Zhao X, Bing W, Meng X, et al. TNF-alpha promotes survival and migration of MSCs under oxidative stress via NF-kB pathway to attenuate intimal hyperplasia in vein grafts. J Cell Mol Med. 2017;21(9):2077–91.
- 33. Hackel A, Aksamit A, Bruderek K, Brandau S. TNF- α and IL-1 β sensitize human MSC for IFN-gamma signaling and enhance neutrophil recruitment. Eur J Immunol. 2021;51(2): 319–30.
- Qian BZ, Li J, Zhang H, Kitamura T, Zhang J, Campion LR, et al. CCL2 recruits inflammatory monocytes to facilitate breasttumour metastasis. Nature. 2011;475(7355):222–5.
- Mak A, Uetrecht J. Involvement of CCL2/CCR2 macrophage recruitment in amodiaquine-induced liver injury. J Immunotoxicol. 2019;16(1):28–33.
- Walens A, DiMarco AV, Lupo R, Kroger BR, Damrauer JS, Alvarez JV. CCL5 promotes breast cancer recurrence through macrophage recruitment in residual tumors. Elife. 2019;8: e43653.
- Lee CM, Peng HH, Yang P, Liou JT, Liao CC, Day YJ. C-C Chemokine Ligand-5 is critical for facilitating macrophage infiltration in the early phase of liver ischemia/reperfusion injury. Sci Rep. 2017;7:3698.
- Kong S, McBurney MW, Fang D. Sirtuin 1 in immune regulation and autoimmunity. Immunol Cell Biol. 2012;90:6–13.
- Wu YJ, Fang WJ, Pan S, Zhang SS, Li DF, Wang ZF, et al. Regulation of Sirt1 on energy metabolism and immune

- response in rheumatoid arthritis. Int Immunopharmacol. 2021; 101:108175.
- Imperatore F, Maurizio J, Vargas Aguilar S, Busch CJ, Favret J, Kowenz-Leutz E, et al. SIRT1 regulates macrophage selfrenewal. EMBO J. 2017;36:2353–72.
- Yang H, Chen J, Chen Y, Jiang Y, Ge B, Hong L. Sirt1 activation negatively regulates overt apoptosis in Mtb-infected macrophage through Bax. Int Immunopharmacol. 2021;91:107283.
- Zhou B, Yang Y, Li C. SIRT1 inhibits hepatocellular carcinoma metastasis by promoting M1 macrophage polarization via NF-κB pathway. Onco Targets Ther. 2019;12:2519–29.
- Isaacs-Ten A, Moreno-Gonzalez M, Bone C, Martens A, Bernuzzi F, Ludwig T, et al. Metabolic regulation of macrophages by SIRT1 determines activation during cholestatic liver disease in mice. Cell Mol Gastroenterol Hepatol. 2022;13:1019–39.
- 44. Liu J, Godlewski G, Jourdan T, Liu Z, Cinar R, Xiong K, et al. Cannabinoid-1 receptor antagonism improves glycemic control and increases energy expenditure through sirtuin-1/mechanistic target of rapamycin complex 2 and 5'Adenosine monophosphateactivated protein kinase signaling. Hepatology. 2019;69:1535–48.
- Ying H, Ying B, Zhang J, Kong D. Sirt1 modulates H3 phosphorylation and facilitates osteosarcoma cell autophagy. Artif Cells Nanomed Biotechnol. 2019;47:3374–81.

How to cite this article: Zong C, Meng Y, Ye F, Yang X, Li R, Jiang J, et al. AIF1⁺CSF1R⁺ MSCs, induced by TNF-α, act to generate an inflammatory microenvironment and promote hepatocarcinogenesis. Hepatology. 2023;78:434–451. https://doi.org/10.1002/hep.32738